On the transient flow behavior in pressurized plastic pipe-based water supply systems

Badreddine Essaidi and Ali Triki

ABSTRACT

Plastic material pipes such as high- or low-density polyethylene (HDPE or LDPE) are increasingly used in new or renewed water supply systems. Therefore, analysis of water hammer surge-waves initiated into such piping systems deserves investigation. The 1-D pressurized-pipe flow model embedding the Ramos formulation was used to describe the flow behavior in the elastic and plastic pipe-based hydraulic system. Numerical computations were performed using the method of characteristics. First, the numerical solver was validated against experimental data, available from the literature. Then, the proposed solver was applied to explore the transient pressure-wave behavior resulting from the power failure to a pumping station. Results evidenced the severity of such a scenario with regards to induced positive and negative pressure-wave magnitudes. Furthermore, the findings of this study suggested that plastic pipe-wall materials allowed a significant attenuation of pressure-wave magnitude in conjunction with the expansion of the pressure-wave oscillation period. It was also found that the observed attenuation and expansion effects depended strongly upon the plastic material type. In this respect, the results revealed that LDPE provided a better trade-off between the two last effects than HDPE.

Key words | design, LDPE/HDPE, power failure, pump, Ramos *et al.* formulation, surge-wave

Badreddine Essaidi
Research Unit: Mechanics, Modelling Energy and Materials M2EM; Department of Mechanical Engineering, National Engineering School of Gabès,
University of Gabès,
Gabès,
Tunisia

Ali Triki (corresponding author)
Higher Institute of Applied Sciences and Technology of Gabès,
University of Gabès,
Gabès,
Tunisia
E-mail: *ali.triki@enis.rnu.tn*

HIGHLIGHTS

- The case of power failure to pump in a water supply system was investigated.
- The Ramos *et al.* formulation was embedded in the waterhammer model to account for the viscoelasticity of the pipe wall and unsteady-friction loss.
- HDPE and LDPE plastic materials –based piping system were investigated.
- Estimate of pressure-wave behavior was validated against experimental data.

NOMENCLATURE

Symbols

a_0	elastic wave-speed (m/s)
a_1, a_2	constants for pump $H - Q$) curve (–)
b_1, b_2	constants for pump ($T - Q$) curve (–)
A	cross-sectional area of the pipe (m^2)
D	internal diameter of the pipe (m)
E_0	Young's modulus of the pipe-wall material (Pa)
e	pipe-wall thickness (m)
g	gravity acceleration (m/s^2)
H	pressure-head (m)
h	dimensionless pressure-head (–)
h_f	pressure-head loss per unit length (–)
I	moment of inertia of the pump ($kg.m^2$)
R_g	radius of gyration of the rotating mass (m)
$k_{r1,}$ k_{r2}	Ramos's unsteady decay coefficients (–)
L	pipe length (m)

doi: 10.2166/aqua.2020.051

N rotational speed of the pump (rpm)
Q average flow-rate (m^3/s)
R resistance coefficient of the pipe (–)
T instantaneous torque of the pump (Nm)
t time (s)
W weight of rotating parts plus entrained liquid (kg)
x coordinate along the pipe centerline (m)
z pipe centerline elevation with respect to pump intake level (m)

Greek symbols

α dimensionless speed ratio (–)
β dimensionless torque ratio (–)
υ dimensionless velocity (–)
Δ time or space step increment (–)
τ valve closure function

Subscripts

0 steady-state/rated value
i section index
ns number of sections
R rated values
(+)/(–) up-/down-surge

Superscripts

i mesh index of the piping system

Acronyms

MOC method of characteristics
HDPE/LDPE high-/low-density polyethylene
1-D-EWHM one-dimensional extended waterhammer model

INTRODUCTION

Water supply systems are frequently subjected to waterhammer surge-waves due to temporal changes in flow conditions at any region in these systems. These changes may be intentional (e.g., startup, stoppage, or control of pump operation, and the setting of their respective valves), or accidental (e.g., failure of power to pumping stations). Waterhammer surge-waves can lead to serious mechanism failure, and can even jeopardize the operator's safety (Besharat *et al.* 2015; Coronado-Hernández *et al.* 2019). Therefore, they should be correctly anticipated in the design stage of water supply systems. Furthermore, the particular transient scenario associated with the failure of power to pumps, also referred to as 'pump failure', needs special consideration, since the hydraulic machine may go through abnormal operation modes during the transient scenario (Donsky 1961; Thorley & Faithfull 1992; Thanapandi & Prasad 1995; Almeida & Ramos 2010; Wan & Zhang 2011; Adamkowski *et al.* 2016; Wan *et al.* 2019). In this regard, the proper analysis of the transient behavior of the hydraulic machine may result in the abandonment of additional surge control devices (e.g., surge tanks) and, hence, may be economically advantageous.

On the other hand, plastic pipes are nowadays preferred to steel and cast-iron ones thanks to their reduced acquisition cost and easy installation, besides their advantageous chemical resistance proprieties. Compared with polyvinyl chloride (PVC), the high- or low-density polyethylene (HDPE or LDPE) is the most widely used. These materials provide a more significant attenuation of transient pressure fluctuations during high- and low-pressure surge loading than elastic ones (Aklonis *et al.* 1972). Physically, this effect is expected due to the viscous properties of plastic materials characterized by a retarded deformation component in conjunction with the immediate one, and observed in the case of elastic materials (such as steel and cast-iron materials). Indeed, during high- and low-pressure-surge loads, the viscoelasticity effects are exhibited by a delayed response of the radial expansion or contraction of the pipe-wall, which results in the magnitude attenuation and the period expansion of the pressure-wave oscillations. Incidentally, several numerical and experimental studies delineated that the visco-elastic properties of plastic pipe-wall materials could be beneficially used for suppressing excessive transient pressure-wave oscillations from water supply systems (Güney 1983; Ghilardi & Paoletti 1986; Triki 2016, 2017, 2018; Fersi & Triki 2019; Triki & Chaker 2019; Trabelsi & Triki 2019, 2020; Chaker & Triki 2020).

From a computational point of view, the analysis of fast transient waves in plastic pipes requires the implementation

of a complete transient solver accounting for unsteady friction loss and non-elastic pipe-wall behavior (Ghidaoui *et al.* 2005; Duan *et al.* 2010; El-Gazzar 2017; Bertaglia *et al.* 2018).

Several approaches have been presented in the literature to enhance both friction losses and pipe-wall material effects which are identified as being the main sources of surge damping. For example, Triki (2017, 2018) used the extended waterhammer solver embedding the Kelvin–Voigt (Aklonis *et al.* 1972) and Vitkovský *et al.* (2000) formulations to account for the pipe-wall viscoelastic behavior and unsteady friction loss, respectively. Incidentally, Triki (2017, 2018) delineated that the combination of the two effects (i.e., pipe-wall viscoelasticity and unsteady friction) leads to a satisfactory agreement between measured data and numerical results. However, the consideration of a single effect could not reproduce experimental results. Subsequently, Ramos *et al.* (2004) introduced an alternative formulation, built upon the Vitkovský *et al.* (2000) approach, coupling the damping effect due to the pipe-wall behavior with the unsteady friction-loss effect. Incidentally, the Ramos *et al.* approach was based on splitting the unique coefficient of the Vitkovsky formulation (k_v) into two distinct decay coefficients, applied to the convective and local acceleration terms in the momentum equation of the classical waterhammer solver. The authors (Ramos *et al.* 2004) verified that these coefficients were practically constant for different Reynold number values. Furthermore, they proved that their numerical solver reasonably reproduced experimental observations with regards to the damping and phase-shift pressure-wave. Compared with the Vitkovsky *et al.* formulation, that of Ramos could characterize unsteady frictions and pipe-wall viscoelastic behavior in simple and rapid implementation. Accordingly, the latter approach will be adopted in this work.

As previously stated, the detailed analysis of waterhammer transients caused by the power failure to pumping stations is crucial in the design stage of water supply systems, which are nowadays increasingly relying on plastic pipe-wall materials. Accordingly, exploration of the transient pressure-wave behavior due to pump failure in a plastic pipe-based water supply system was planned in this paper.

The following section outlines the discretization of the Ramos *et al.* formulation-based one-dimensional extended waterhammer model (1-D-EWHM) using the method of characteristics (MOC).

METHODOLOGY

The 1-D-EWHM introduced by Ramos *et al.* (2004) may be expressed as follows:

$$\frac{\partial H}{\partial t}+\frac{a_0^2}{gA}\frac{\partial Q}{\partial x}=0 \text{ and } \frac{1}{A}\frac{\partial Q}{\partial t}+g\frac{\partial H}{\partial x}+gh_f=0 \tag{1}$$

where, H = pressure-head; Q = discharge; A = pipe-area; g = acceleration due to gravity; $a_0=\sqrt{K/\rho/1+[\alpha(D/e)K]/E_0}$ = elastic-wave-speed; K = bulk elasticity modulus of the fluid ($K=2.19$ GPa for water); ρ = fluid mass density ($\rho=999$ kg/m^3 for water); α = dimensionless parameter describing pipe constraint condition ($\alpha=1.04$, for thin-wall elastic pipes (Wylie *et al.* 1993)); D = internal pipe diameter; e = pipe-wall thickness; E_0 = Young's modulus of the pipe-wall material; $h_f=(h_{f_s}+h_{f_u})$ = pressure-head loss per unit length; h_{f_s} = quasi-steady pressure-head-loss component per unit length ($h_{f_s}=fQ|Q|/(2DA)$ or $h_{f_s}=32\nu' Q/(gD^2A)$, for turbulent or laminar flow, respectively); f = Darcy–Weisbach friction factor; ν' = kinematic fluid viscosity; $h_{f_u}=\{k_{r1}\partial Q/\partial t+k_{r2}a_0\,\mathrm{sgn}(Q)|\quad \partial Q/\partial x|\}/\{gA\}$ = unsteady pressure damping (Ramos *et al.* 2004; Szymkiewicz & Mitosek 2014); k_{r1}, k_{r2} = decay coefficients, affecting the phase-shift and damping of the transient pressure wave, respectively ($k_{r1}=0.003$ and $k_{r2}=0.04$ for plastic material); sgn = operator for the sign of the discharge; t = time, and x = distance along the pipe centerline axis.

The numerical solution of the 1-D-EWHM (1) is commonly derived using the MOC.

Briefly, the MOC applied to the above pressure transient problem at any grid point (i, t) (Figure 1), can be described by the following finite difference expressions (details are reported in, for example, Wylie *et al.* (1993), Ramos *et al.* (2004), Afshar & Rohani (2008), Soares *et al.* (2013), Chaudhry (2014), Triki (2016), Triki & Fersi (2018) and Fersi & Triki (2019):

$$C_{\pm}:\ \frac{dQ}{dt}+\frac{gA}{\alpha_{\pm}\times(1+k_r1)}\frac{dH}{dt}+\frac{f}{2d(1+k_r1)}Q|Q| = 0 \ \text{ along } \frac{dx}{dt}=\alpha_{\pm} \tag{2}$$

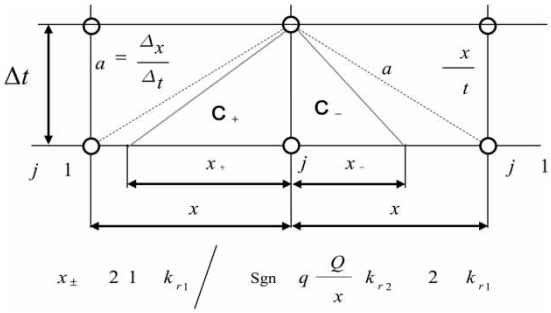

Figure 1 | Characteristics lines in the ($x - t$) plane, for the Ramos *et al.* formulation.

where, $\alpha_{\pm} = 2a_0(1 + k_r1)/\left(-\text{sgn}\left(Q\frac{\partial Q}{\partial x}\right)k_r2 \pm (2 + k_r1)\right)$, and sgn = operator for the 'sign'.

The compatibility equations associated with the finite difference form (2) may be written as:

$$C^i_{\pm}: \begin{cases} Q_{i,t} = c_P - c_a H_{i,t} \\ Q_{i,t} = c_N + c_a H_{i,t} \end{cases} \tag{3}$$

where, $c_P = Q_{i-1,t-\Delta t} + c'_P H_{i-1,t-\Delta t} - c_P/1 + k_r1$; $c'_P = c_a/\alpha_+$; $c_a = gA/a_0$; $c_P = R \times A \times \Delta t \times Q_{i+1,t} - |Q_{i+1,t}|$; $c_N = Q_{i+1,t} + c'_N H_{i+1,t} + c_N/1 + k_r1$; $c'_N = c_a/\alpha_-$; $c_N = RAQ_{j+1,t}$; $R = f/(2DA)$; i = pipe section number $(1 \le j \le n_s)$; n_s = pipe sections number; Δx = space step; and Δt = time step.

In order to proceed further, it is necessary to stipulate boundary conditions. The conditions used for this study include the following.

(i) Power loss to a pump upstream:

The major problem in this case consists in the handling of pump characteristics and the resulting boundary conditions at the suction and discharge junctions of the pumping station. Principally, four parameters are required for the mathematical characterization of the pump behavior and including the discharge Q, the pressure-head H, the rotational speed N of the pump, and the net shaft-torque T. These parameters are commonly utilized in a dimensionless form relative to the rated values benchmark (i.e., $\upsilon = Q/Q_R$, $h = H/H_R$, $\alpha = N/N_R$, and $\beta = T/T_R$, respectively). They are characterized basing on the Suter's head and torque curves which are generally collected for different specific speeds (i.e., $F_h = \{h/(\upsilon^2 + \alpha^2)\}$ and $F_b = \{\beta/(\upsilon^2 + \alpha^2)\}$ vs $\theta = \tan^{-1}(\alpha/\upsilon)$).

For the numerical computation procedure, these parameters are first stored for equal increments $\Delta\theta$, and subsequently evaluated at each time step using an iterative procedure:

$$\begin{aligned} h/(\alpha^2 + \upsilon^2) &= a_1 + a_2\tan^{-1}(\alpha/\upsilon) \\ \beta/(\alpha^2 + \upsilon^2) &= b_1 + b_2\tan^{-1}(\alpha/\upsilon) \end{aligned} \tag{4}$$

The boundary equations describing the pump failure condition may be established according to Figure 2.

First, the characteristics equations C_+ and applied at the nodes a and c, respectively, are written as:

$$F_a = Q - c_P + c_a H = 0 \tag{5}$$

$$F_c = Q - c_N - c_a H = 0 \tag{6}$$

Second, the pressure-head balance relationship across the pump (2) may be expressed as follows:

$$H_a + H = H_b \tag{7}$$

where, H = total dynamic head across the pump, which is determined from the dimensionless-homologous relationships (4). Then, Equation (7) becomes:

$$H_a - H_b + H_R(\upsilon^2 + \alpha^2)(a_1 + a_2\tan^{-1}(\alpha/\upsilon)) = 0 \tag{8}$$

Third, the pressure-head loss across the check-valve (3) may be evaluated as:

$$F_3 = H_b - H_c - \frac{Q \times |Q|}{c_v} = 0 \tag{9}$$

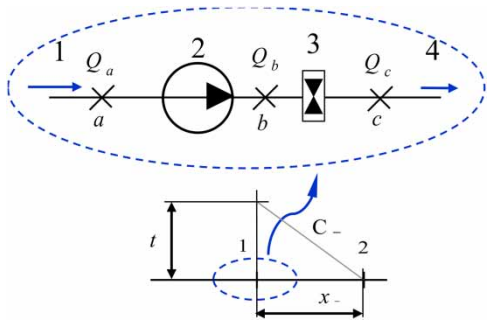

Figure 2 | Schematic illustration of the pump and its control valve at the upstream extremity (node 1) [(1,4) flow; (2) pump; (3) check-valve].

where, $c_v = Q_R^2 \times \tau/(2 \times \Delta H_0) =$ coefficient of pressure-head at the valve head loss, and $\tau =$ prescribed valve position.

Fourth, the decelerating torque resulting from the power failure is evaluated as:

$$F_T = \beta + \beta_0 - c_T(\alpha_0 - \alpha) \tag{10}$$

in which: $c_T = I \times (N_R/T_R) \times (\pi/30\Delta t)$; $I = W \times R_g^2/g =$ combined polar moment of inertia of the pump, motor, shaft, and liquid entrained in the pump impeller; $W =$ weight of rotating parts and the entrained liquid; $R_g =$ radius of gyration of the rotating mass; α and $\beta =$ average values of the dimensionless rotational speed N and net torque T during the time step Δt, and the subscript 'zero' corresponding to the values two time steps earlier. Incidentally, these average values α and β may be determined from the Suter curves using a parabolic interpolation.

Subsequently, the combination of Equation (8) with Equations (5)–(7), leads to:

$$F_h = H_R(\upsilon^2 + \alpha^2)(a_1 + a_2 x) + \frac{\alpha_+}{c_p}(c_N - \upsilon Q_R) - \frac{\upsilon \times |\upsilon| \Delta H_0}{\tau^2} = 0 \tag{11}$$

Besides, the combination of Equations (10) and (4) yields:

$$F_T = (\upsilon^2 + \alpha^2)(b_1 + b_2 x) + -\beta_0 - c_T(\alpha_0 - \alpha) = 0 \tag{12}$$

Finally, Equations (11) and (12) are solved for α and υ using a Newton–Raphson method-based numerical procedure.

Incidentally, the pressure-head value at the upstream extremity may be determined from the backward characteristic equation C_.

(ii) Constant level reservoir downstream:

This condition is expressed using the following equation:

$$H_{n_s,t+\Delta t} = H_{t=0}^{\text{Res.}} \tag{13}$$

where, $H_{t=0}^{\text{Res.}}$ is the elevation of the reservoir surface above the reference datum.

Besides, the discharge value is determined using the forward characteristic equation C_+.

To ascertain the validity of the developed MOC-based algorithm, the numerical solution is then compared with experimental data available from the literature.

MODEL VALIDATION

First, data from laboratory experiments, conducted by Ramos *et al.* (2004), are used to validate the developed numerical model, within a reservoir-high-performance-polyethylene-pipe-valve system whose characteristics are: length $L = 100$ m, diameter $D = 44$ mm, and wave-speed $a_0 = 330.0$ m/s. The initial steady-state regime corresponds to a discharge value $Q_0 = 1.81l/s$. Experimental data relate to a transient flow regime initiated by the rapid closure of the downstream valve.

Figure 3 provides a comparison of measured and numerical results computed from the 1-D-EWHM based on the Ramos *et al.* (2004) or the Vitkovský *et al.* (2000) formulations.

At first glance, it illustrates clearly that the wave signal computed based on the Ramos *et al.* formulation agrees

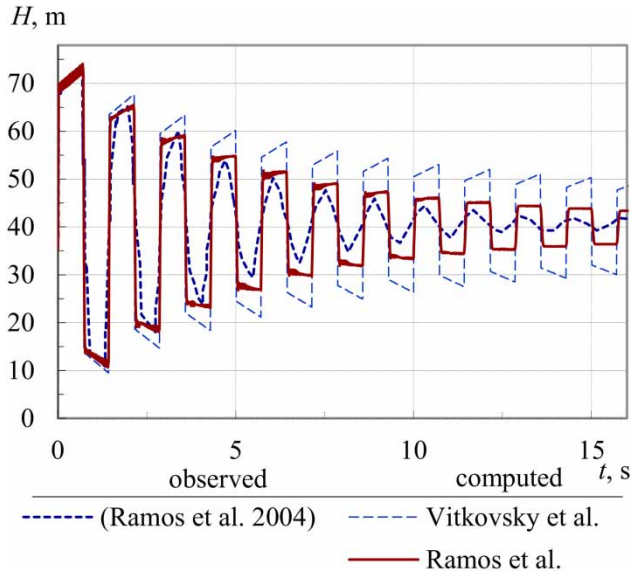

Figure 3 | Comparison of pressure-head signals obtained from experimental observations and numerical computations using the Vitkovsky *et al.* ($k_v = 0.03$) or Ramos *et al.* ($k_{r1} = 0.003/k_{r2} = 0.04$) formulations.

well with the observed one, with regard to the magnitude and phase-shift, for the first and second cycles of pressure-head-wave oscillations. Contrarily, it suggests that the magnitude of the pressure-wave signal computed using the Vitkovsky *et al.* formulation exceeds the observed one. This, in turn, suggests that the use of two separate weighting coefficients (i.e., k_{r1} and k_{r2}), instead of a single one (i.e., k_v), improved, significantly, the prediction accuracy of the unsteady friction and damping effects on the plastic pipe.

Second, the numerical solution is compared with the Hollander experimental data measured at the California Institute of Technology (Streeter & Wylie 1967). The hydraulic system consists of two identical centrifugal pumps in parallel ($Q_R = 21.72$ m^3/s, $H_R = 60$ m, $N_R = 180$ rpm, $W \times R_g^2 = 1670$ Kg m^2, and dimensionless-homologous head and torque curves for the pump-specific speed $N_S = 34.8$ rpm in Figure 4, as taken from Streeter & Wylie's data) discharging in a single common buried concrete pipe ($L = 1564$ m, $D = 4.75$ m). The experimental test conducted by Hollander corresponds to the simultaneous failure of both pumps.

Figure 5 compares the dimensionless pressure-head and speed signals recorded by Hollander and their counterparts provided by the numerical solution. It shows acceptable

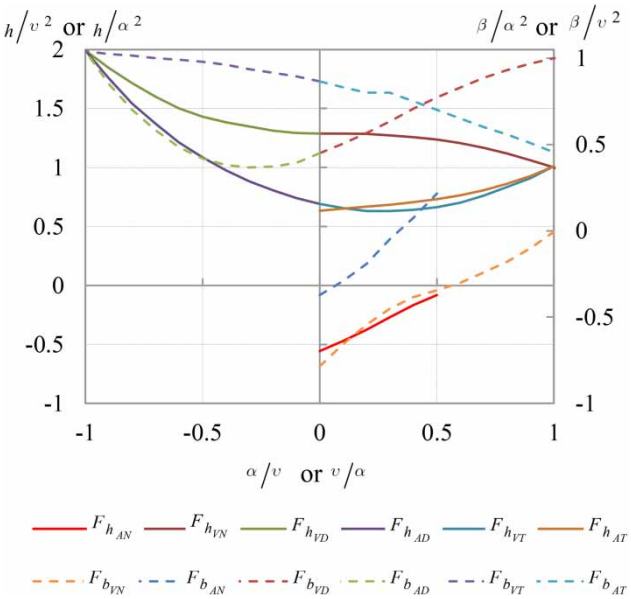

Figure 4 | Dimensionless-homologous head and torque data for the specific speed $N_S = 34.8$ rpm : [subscripts *A* or $V = h/v^2$.vs α/v or h/α^2.vs v/α, respectively; and subscripts *N*, *D*, or *T* = normal, energy dissipation, or turbine operation zones, respectively].

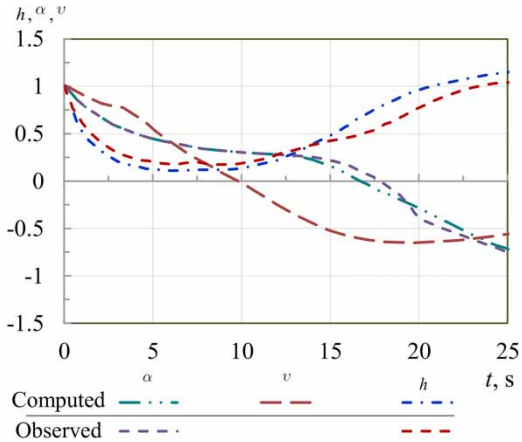

Figure 5 | Comparison of computed and observed dimensionless pressure-head, velocity, and speed signals.

agreement between experimental and computed signals within the normal operation zone of the hydraulic machine (i.e., $\alpha \succ 0$ and $v \succ 0$). However, discrepancies appear between measured and computed results in the turbine zone (i.e., $\alpha \prec 0$ and $v \prec 0$). As per Streeter & Wylie (1967) and Wylie *et al.* (1993), these discrepancies are associated with the assumed pump characteristic data which are available only for the normal operating zone of the hydraulic machine.

In the following section, the developed solver is implemented to describe the waterhammer wave behavior initiated by the power failure to a pumping system.

CASE STUDY

The test case, considered in this study, relates to the pumping system shown in Figure 6. The elevation of the upstream reservoir above the downstream one is equal

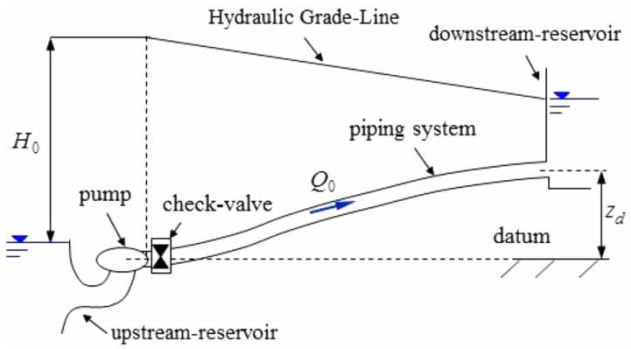

Figure 6 | Hydraulic system layout.

to: $z_d = 83.8$ m. The pipe and pump characteristics are summarized in Table 1, and the Suter's head and torque curves, corresponding to the pump-specific speed $N_S = 25$ rpm, are plotted in Figure 7. Initially, the pump operates at rated conditions, and the transient regime is caused by the failure of power to the upstream pump. Meanwhile, the check-valve begins to close after 1.5 s.

To highlight the effect of the pipe-wall material on the transient pressure-surge behavior, the steel, HDPE and LDPE materials are addressed in this study ($E_0^{\mathrm{STEEL}} = 152.0$ GPa, $E_0^{\mathrm{HDPE}} = 1.43$ GPa or $E_0^{\mathrm{LDPE}} = 0.648$ GPa, respectively (Keramat & Haghighi 2014)).

In the following, the characteristics of positive and negative pressure-surges are denoted by the symbols (+) and (−), respectively. Besides, indicators linked to the first cycle of pressure-wave oscillations are used to interpret different attributes of the pressure-head signals, including: (i) the magnitude of positive or negative pressure-surges: $\Delta h^{\pm} = h^{\max/\min} - h_0$; (ii) the attenuations of positive and negative pressure-surge magnitudes involved by the HDPE or LDPE material-based piping system relatively to those corresponding to the steel material-based system: $\delta h^{\pm}_{\mathrm{HDPE/LDPE}} = \Delta h^{\pm}_{\mathrm{STEEL}} - \Delta h^{\pm}_{\mathrm{HDPE/LDPE}}$; (iii) the phase-shift between the pressure-wave oscillation signals performed by an HDPE or LDPE material-based pipe and the signal involved by a steel material pipe: $\delta T^1_{\mathrm{HDPE/LDPE}} = (T^1_{\mathrm{HDPE/LDPE}} - T^1_{\mathrm{STEEL}})$; and (iv) the ratios between the relative attenuation of positive or negative pressure-surge and the phase-shift: $\eta^{\pm}_{\mathrm{HDPE/LDPE}} = \delta h^{\pm}_{\mathrm{HDPE/LDPE}} / \delta T^1_{\mathrm{HDPE/LDPE}}$.

Figure 8(a)–8(c) illustrate, respectively, the dimensionless pressure-head signals and valve position, the dimensionless velocity and speed signals, predicted at the upstream extremity of the piping system, and the zones of pump operation during the transient process involved by steel, HDPE or LDPE materials-based piping systems.

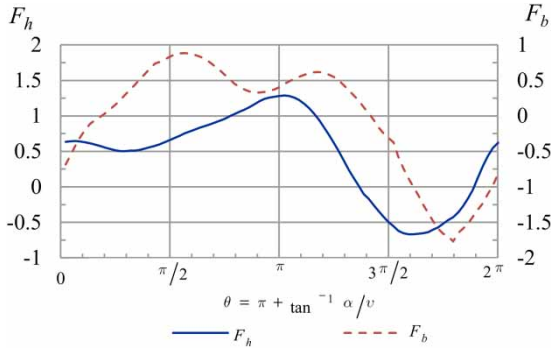

Figure 7 | Suter's curves for the specific speed $N_s = 25$ rpm.

Jointly, the main features of the pressure-head signals displayed in Figure 8(a) are listed in Table 2.

At first glance, the general wave pattern of Figure 8 indicates that the flow rapidly diminishes to zero and then reverses (Figure 8(b)). As the pump rapidly loses its forward rotation and reverses shortly after the flow reversal, a negative pressure-wave is propagated downstream from the pump (Figure 8(a)) and a positive pressure-wave is propagated upstream through the suction pipe. As the pump increases in speed in the reverse direction, it causes greater resistance to flow, which produces a high pressure in the discharge line (Figure 8(a)).

On the other hand, Figure 8(a) clearly illustrates expanded values of the wave oscillation periods involved in plastic pipe-based hydraulic systems as compared with their counterpart observed in a steel pipe-based system. Overall, the magnitudes of positive and negative pressure-surges and the values of wave oscillation periods depend on the pipe-wall material used for the piping system.

Referring to Figure 8(a)–8(c) and the data listed in Table 2, the following interpretations may be carried out for the first cycle of pressure-wave oscillations.

First, Figure 8(a) and Table 2 suggest that the larger positive and negative pressure-head magnitudes are involved

Table 1 | Characteristics of the piping system in Figure 6

Pipe					
Parameters	L [m]	D [mm]	f [-]	a_0 [m/s]	Q [m^3/s]
Value	550	0.75	0.02	1,067	0.178
Pump					
Parameters	Q_R [m^3/s]	H_R [m]	T_R [kg.m]	N_R [rpm]	I [kg.m^2]
Value	0.178	94.5	99.0	147.0	7.88

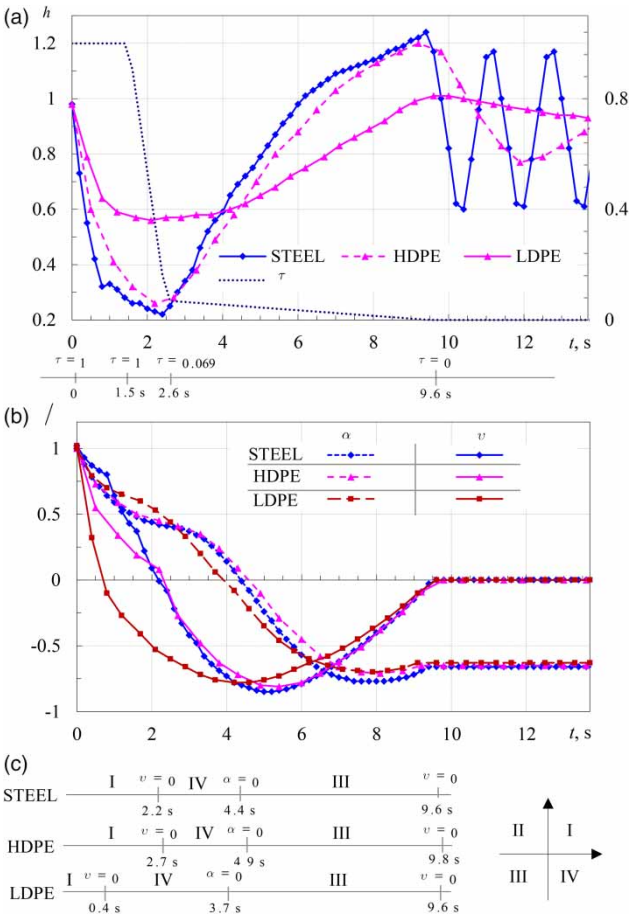

Figure 8 | Dimensionless (a) pressure-head and valve position; (b) velocity and speed; and (c) zones of pump operation (I = normal, II = reversed speed dissipation, III = turbine, and IV = dissipation zones).

Table 2 | Characteristics of pressure-wave traces in Figure 8

Pipe-wall material	Period (s)	h^{max} (–)	h^{min} (–)
Steel	9.80	1.24	0.22
HDPE	10.30	1.20	0.26
LDPE	11.60	1.05	0.50

by the case utilizing a steel pipe: $\Delta h^{+}_{\mathrm{STEEL}} = 0.3$ and $\Delta h^{-}_{\mathrm{STEEL}} = 0.8$, respectively. Inversely, this case involves the shorter wave oscillation period: $T^{1}_{\mathrm{STEEL}} = 9.8$ s.

On the other hand, concerning the operating zones of the hydraulic machine during the transient process, Figure 8(c) shows that the machine operates in the normal pump zone (i.e., zone I $\alpha \succ 0$ and $\upsilon \succ 0$) up to $t = 2.2$ s, and then operates in the dissipation zone (zone IV) up to $t = 4.4$ s due to flow reversal ($\upsilon \prec 0$), while the inertia of the rotating parts maintains a positive rotation ($\alpha \geq 0$). Subsequently, the hydraulic machine experiences reversal in both flow and rotational speed (i.e., $\alpha \prec 0$ and $\upsilon \prec 0$) beyond the time $t = 4.4$ s. In this case, the machine operates in the turbine zone (zone III).

Second, Figure 8(a) and Table 2 demonstrate that the HDPE material-based piping system case leads to less important magnitudes of positive and negative pressure-head surges and a more important wave oscillation period compared with the case utilizing a steel pipe. Specifically, the relative attenuations of positive and negative pressure-surge magnitudes, depicted between the HDPE material-based piping system and the steel material-based one, are equal to: $\delta h^{\pm}_{\mathrm{HDPE}} = \mp 0.40$. Also, the phase-shift induced between the latter two cases is equal to: $\delta T^{1}_{\mathrm{HDPE}} = 0.50$ s. These results, in turn, imply the ratios between the relative attenuation of positive and negative pressure-surges and the phase-shift: $\eta^{\pm}_{\mathrm{HDPE}} = \mp 0.08\ \mathrm{s}^{-1}$.

Concerning the operating zones of the hydraulic machine involved in this case, Figure 8(b) and 8(c) indicate that the machine operates in the normal pumping zone (zone I) during $0 \leq t \leq 2.7$ s; and, subsequently, in the dissipation zone (zone IV) up to $t = 4.4$ s. Thereafter, the machine operates in the turbine zone (zone III).

Third, Figure 8(a) and Table 2 show that the LDPE material-based piping system case leads to less important magnitudes of positive and negative pressure-head surges and a more important wave oscillation period compared with the case utilizing a steel pipe. Specifically, the relative attenuations of positive and negative pressure-surge magnitudes, depicted between the LDPE and steel setup-based piping systems, are equal to: $\delta h^{+}_{\mathrm{LDPE}} = -0.19$ and $\delta h^{-}_{\mathrm{LDPE}} = 0.3$, respectively. In addition, the phase-shift induced between the two latter cases is equal to: $\delta T^{1}_{\mathrm{LDPE}} = 0.28$ s. These results involve the ratios between the relative attenuation of positive and negative pressure-surges and the phase-shift: $\eta^{+}_{\mathrm{LDPE}} = -0.11\ \mathrm{s}^{-1}$ and $\eta^{-}_{\mathrm{LDPE}} = 0.16\ \mathrm{s}^{-1}$, respectively.

Incidentally, it should be pointed out here that the LDPE setup-based piping system leads to more important attenuations of positive and negative pressure-surge magnitudes, and more expansion of pressure-wave oscillation period,

than the one employing an HDPE material. Interestingly, the LDPE setup provides a larger ratio than HDPE ($\eta^{+}_{\mathrm{LDPE}} \succ \eta^{+}_{\mathrm{HDPE}}$ and $\eta^{-}_{\mathrm{LDPE}} \succ \eta^{+}_{\mathrm{HDPE}}$). This implies that the LDPE setup provides a more important attenuation accompanied with a less important expansion of pressure-wave signal than the HDPE setup-based piping system. Thereupon, it may be concluded that the LDPE material-based piping system case allows a better trade-off between the attenuations of positive and negative pressure-surge magnitudes and the expansion of the pressure-wave oscillation period compared with the case using an HDPE material.

Regarding the operating zones of the hydraulic machine involved in this case (i.e., LDPE piping system), Figure 8(b) and 8(c) indicate that the machine operates in the normal pumping zone (zone I) during $0 \leq t \leq 2.7$ s and, subsequently, in the dissipation zone (zone IV) up to $t = 4.4$ s. Thereafter, the machine operates in the turbine zone (zone III).

CONCLUSION

Ultimately, this study suggests that the use of a plastic pipe-wall material-based pumping system provides a large attenuation effect of the first pressure-head rise and drop, associated with an expansion effect of the period of pressure-wave oscillations, for a pump failure-initiated transient scenario. In addition, the pressure attenuation and period expansion effects are pronounced when using an LDPE pipe-wall material compared with an HDPE material. Specifically, results indicate that the LDPE material allows a better trade-off between the two last effects than HDPE.

Although the present work addressed a particular procedure for valve closure, future investigations on the dependency of the transient pressure-wave behavior upon the check valve setting modes may represent an extension to this study, in particular the determination of the optimal valve closure procedure.

CONFLICT OF INTEREST

The authors declare that there is no conflict of interest.

DATA AVAILABILITY STATEMENT

All relevant data are included in the paper or its Supplementary Information.

REFERENCES

Adamkowski, A., Henke, A. & Lewandowski, M. 2016 Resonance of torsional vibrations of centrifugal pump shafts due to cavitation erosion of pump impellers. *Engineering Failure Analysis* **70**, 56–72. doi:10.1016/j.engfailanal.2016.07.011.

Afshar, M. H. & Rohani, M. 2008 Water hammer simulation by implicit method of characteristic. *International Journal of Pressure Vessels and Piping* **85** (12), 851–859. doi:10.1016/j.ijpvp.2008.08.00.

Aklonis, J. J., MacKnight, W. J. & Shen, M. 1972 *Introduction to Polymer Viscoelasticity*. Wiley-Interscience, New York, USA.

Almeida, A. B. & Ramos, H. M. 2010 Water supply operation: diagnosis and reliability analysis in a Lisbon pumping system. *Journal of Water Supply: Research and Technology-AQUA* **59** (1), 66–78. doi:10.2166/aqua.2010.051.

Bertaglia, G., Ioriatti, G. M., Valiani, A., Dumbser, M. & Caleffi, V. 2018 Numerical methods for hydraulic transients in visco-elastic pipes. *Journal of Fluids and Structures* **81**, 230–254. doi:10.1016/j.jfluidstructs.2018.05.004.

Besharat, M., Tarinejad, R. & Ramos, H. 2015 The effect of water hammer on a confined air pocket towards flow energy storage system. *Journal of Water Supply: Research and Technology - AQUA* **65** (2), 116–126. doi.:10.2166/aqua.2015.081.

Chaker, M. A. & Triki, A. 2020 The branching redesign technique used for upgrading steel-pipes-based hydraulic systems: re-examined. *Journal of Pressure Vessel Technology* **143** (3). doi:10.1115/1.4047829.

Chaudhry, M. H. 2014 *Applied Hydraulic Transients*, 3rd edn. Van Nostrand Reinhold Co, New York, USA. doi:10.1007/978-1-4614-8538-4_4.

Coronado-Hernández, O. E., Besharat, M., Fuertes-Miquel, V. S. & Ramos, H. M. 2019 Effect of a commercial air valve on the rapid filling of a single pipeline: a numerical and experimental analysis. *Water* **11** (9), 1814. doi.:10.3390/w11091814.

Donsky, B. 1961 Complete pump characteristics and the effects of specific speeds on hydraulic transients. *Journal of Basic Engineering* **83** (4), 685–696. doi:10.1115/1.3662299.

Duan, H. F., Ghidaoui, M., Lee, P. J. & Tung, Y.-K. 2010 Unsteady friction and visco-elasticity in pipe fluid transients. *Journal of Hydraulic Research* **483**, 354–362. doi:10.1080/00221681003726247.

El-Gazzar, D. M. 2017 Finite element analysis for structural modification and control resonance of a vertical pump. *Alexandria Engineering Journal* **56** (4), 695–707. doi:10.1016/j.aej.2017.02.018.

Fersi, M. & Triki, A. 2019 Investigation on re-designing strategies for water-hammer control in pressurized-piping systems. *Journal of Pressure Vessel Technology* **141** (2), 021301. doi: 10.1115/1.4040136.

Ghidaoui, M. S., Zhao, M., McInnis, D. A. & Axworthy, D. H. 2005 A review of water hammer theory and practice. *Applied Mechanics Review* **58** (1), 49–76. doi: 10.1115/1.1828050.

Ghilardi, P. & Paoletti, A. 1986 Additional viscoelastic pipes as pressure surge suppressors. In: *Proceedings of 5th International Conference on Pressure Surges*, Hannover, Germany, pp. 113–121.

Güney, M. S. 1983 Waterhammer in viscoelastic pipes where cross-section parameters are time dependent. In: *Proc. 4th Int. Conf. on Pressure Surges*, BHRA, Bath, UK, pp. 189–209.

Keramat, A. & Haghighi, A. 2014 Straightforward transient-based approach for the creep function determination in viscoelastic pipes. *Journal of Hydraulic Engineering* **140** (12). doi:10.1061/(ASCE)HY.1943-7900.0000929.

Ramos, H., Covas, D., Borga, A. & Loureiro, D. 2004 Surge damping analysis in pipe systems: modelling and experiments. *Journal of Hydraulic Research* **42** (4), 413–425.

Soares, A. K., Covas, D. & Ramos, H. M. 2013 Damping analysis of hydraulic transients in pump-rising main systems. *Journal of Hydraulic Engineering* **13** (92). doi:10.1061/(ASCE)HY.1943-7900.0000663.

Streeter, V. L. & Wylie, E. B. 1967 *Hydraulic Transients*. Prentice-Hall, Englewood Cliffs, NJ, USA.

Szymkiewicz, R. & Mitosek, M. 2014 Alternative convolution approach to friction in unsteady pipe flow. *Journal of Fluids Engineering* **136** (1), 011202. doi:10.1115/1.4025509.

Thanapandi, P. & Prasad, R. 1995 Centrifugal pump transient characteristics and analysis using the method of characteristics. *International Journal of Mechanical Sciences* **37** (1), 77–89. doi:10.1016/0020-7403(95)93054-A.

Thorley, A. R. D. & Faithfull, E. M. 1992 Inertias of pumps and their driving motors. In: *Proceedings of the International Conference on Unsteady Flow and Fluid Transients* (R. Bettess & J. Watts, eds). Balkema, Rotterdam, Netherlands, pp. 285–289.

Trabelsi, M. & Triki, A. 2019 Dual control technique for mitigating water-hammer phenomenon in pressurized steel-piping systems. *International Journal of Pressure Vessels and Piping* **172**, 379–413. doi:10.1016/j.ijpvp.2019.04.011.

Trabelsi, M. & Triki, A. 2020 Exploring the performances of the dual technique-based water-hammer redesign strategy in water-supply systems. *Journal of Water Supply: Research and Technology-AQUA* **69**, 6–17. doi:10.2166/aqua.2017.073.

Triki, A. 2016 Water-hammer control in pressurized-pipe flow using an in-line polymeric short-section. *Acta Mechanica* **227** (3), 777–793. doi:10.1007/s00707-015-1493-13.

Triki, A. 2017 Water-hammer control in pressurized-pipe flow using a branched polymeric penstock. *Journal of Pipeline Systems Engineering and Practice* **8** (4), 04017024. doi:10.1061/(ASCE)PS.1949-1204.0000277.

Triki, A. 2018 Further investigation on water-hammer control inline strategy in water-supply systems. *Journal of Water Supply: Research and Technology-AQUA* **67** (1), 30–43. doi:10.2166/aqua.2017.073.

Triki, A. & Chaker, M. A. 2019 Compound technique-based inline design strategy for water-hammer control in steel pressurized-piping systems. *International Journal of Pressure Vessels Piping* **169**, 188–203. doi:10.1016/j.ijpvp.2018.12.001.

Triki, A. & Fersi, M. 2018 Further investigation on the water-hammer control branching strategy in pressurized steel-piping systems. *International Journal of Pressure Vessels Piping* **165**, 135–144. doi:10.1016/j.ijpvp.2018.06.002.

Vítkovský, J. P., Lambert, M. F. & Simpson, A. R. 2000 Advances in unsteady friction modelling in transient pipe flow. In: *Proceedings of the 8th International Conference on Pressure Surges – Safe Design and Operation of Industrial Pipe Systems* (A. Anderson ed.). Publication No. 39, BHR Group, Suffolk, UK, pp. 471–498.

Wan, W. & Zhang, B. 2011 Investigation on complete characteristics and hydraulic transient of centrifugal pump. *Journal of Mechanical Sciemce and Technology* **25**, 2583. doi:10.1007/s12206-011-0729-9.

Wan, W., Zhang, B. & Chen, X. 2019 Investigation on water hammer control of centrifugal pumps in water supply pipeline systems. *Energies* **12** (1), 108. doi:10.3390/en12010108.

Wylie, E. B. & Streeter, V. L. with Lisheng, S. 1993 *Fluid Transients in Systems*. Prentice Hall, Englewood Cliffs, NJ, USA.

First received 1 June 2020; accepted in revised form 14 September 2020. Available online 19 November 2020